The Astrophysical Journal, 659:1352–1359, 2007 April 20

HUBBLE SPACE TELESCOPE MEASUREMENTS OF VACUUM ULTRAVIOLET LINES OF INTERSTELLAR CH

Y. Sheffer and S. R. Federman
Department of Physics and Astronomy, University of Toledo, Toledo, OH 43606; ysheffe@utnet.utoledo.edu, steven.federman@utoledo.edu
Received 2006 September 24; accepted 2007 January 12

ABSTRACT

Three interstellar absorption lines near 1370 Å seen toward ζ Oph have been assigned by Watson to Rydberg transitions in the *G–X* (or 3*d–X*) band of CH. Our survey of a dozen diffuse interstellar lines of sight shows that the three absorption lines are consistent with the known column densities of CH, by deriving the following oscillator strengths: $f(1368.74) = 0.019 \pm 0.003$, $f(1369.13) = 0.030 \pm 0.005$, and $f(1370.87) = 0.009 \pm 0.001$. We also determined intrinsic line widths that correspond to decay rates of $(1.5 \pm 0.6) \times 10^{11}$, $(3.8 \pm 0.7) \times 10^{11}$, and $(1.1 \pm 0.6) \times 10^{10}$ s^{-1} for λλ1368, 1369, and 1370, respectively. These rates are significantly higher than those associated with radiative decays and, thus, are readily attributable to predissociation of the Rydberg state. A fourth interstellar line near 1271 Å has been conjectured by Watson to be the strongest transition in the 4*d–X* Rydberg band of CH. We detected this line along four sight lines and our spectrum syntheses show that with $f(1271.02) = 0.007 \pm 0.002$, it is also consistent with the known column densities of CH. In addition, we conducted a search for the *F–X* band of CH near 1549 Å, and successfully discovered two of its absorption features along four sight lines. The astronomical oscillator strengths derived for these features are $f(1549.05) = 0.021 \pm 0.006$ and $f(1549.62) = 0.013 \pm 0.003$. Finally, the X Per sight line provided us with an astronomical detection of another CH band via two *D–X* features near 1694 Å. Comparisons with results of available theoretical calculations for the four CH bands are presented.

Subject headings: ISM: lines and bands — ISM: molecules — molecular data — ultraviolet: ISM

1. INTRODUCTION

The first listing of three unidentified (UID) features around 1369 Å and along the "classic" diffuse interstellar sight line toward ζ Oph was provided by Cardelli et al. (1991). Their listing included two lines at 1368.74 and 1370.87 Å, as well as the feature at 1369.13 Å, which according to their remark, resembled a diffuse interstellar band (DIB) by virtue of its uncommon larger and asymmetric width. This proposition was studied further by Tripp et al. (1994), who introduced the UID1 through UID3 nomenclature for these features and suggested that UID2 at 1369.13 Å is probably the first ultraviolet (UV) analog of the optical DIBs. Gnaciński et al. (1997) showed that as far as equivalent width (W_λ) is concerned, UID2 has a better correlation with W_λ(CO) than with W_λ(Ni II), or with H I and Na I column densities (N) along six diffuse sight lines. Their conclusion was that UID2 most probably arises in a denser, molecular medium.

Watson (2001) performed a rigorous reanalysis of room-temperature laboratory data of CH that was published by Herzberg & Johns (1969). He showed that an assignment of the UID trio observed toward ζ Oph to CH is very plausible on the grounds of wavelength coincidence and approximate intensity or transition strengths. Specifically, the assignment was to the *G–X* band of CH, which was first observed in the laboratory by Herzberg & Johns, who classified it as the first member ($n = 3$) of the *nd* Rydberg series. Moreover, the defining characteristic of UID2, it being appreciably wider than other UID and identified absorption lines, could be explained as arising from heterogeneous predissociation of the Rydberg states of CH, including the $G(^2\Sigma^+, {}^2\Pi, {}^2\Delta)$, or 3*d*, complex of three states. The phenomenon of prominent Lorentzian wings signaling the extremely short lifetime of the upper state is well known in Rydberg transitions of, e.g., CO (Viala et al. 1988; Eidelsberg et al. 2006), when closely spaced rotational lines blend into each other more strongly in bands that arise from states with faster predissociation rates, or wider wings.

Here we show that an identification of the UID features around 1369 Å with 3*d–X* Rydberg transitions in CH is consistent with the expected range of *f*-values and with known N(CH) values, as well as with line broadening arising from predissociation. This is accomplished by using profile synthesis to model the observed line shapes and absorption strengths in high-resolution (high-*R*) *Hubble Space Telescope* (*HST*) spectra. Furthermore, we were able to detect and analyze the λ1271 UID feature introduced by Federman et al. (1995) which Watson (2001) conjectured to be the strongest transition in the 4*d–X* band, the second member in the *nd* Rydberg series of CH (Herzberg & Johns 1969). Indeed, our spectral syntheses show that this UID is also consistent with theoretical predictions for the band *f*-value, and with observed values of N(CH).

Finally, we conducted a deliberate search for additional spectral signatures of CH based on the previous laboratory work of Herzberg & Johns (1969). According to their Table 15, the bands *D–X* at 1694 Å, *E–X* at 1557 Å, and *F–X* at 1549 Å may be detected in the interstellar medium via their vacuum UV (VUV) transitions from a Λ-component of the $J'' = 1/2$ level of the $X\ ^2\Pi$ ground state. Our search resulted in positive detections of the *F–X* and the *D–X* bands, but none of the *E–X* band.

A note concerning spectroscopic notation and molecular predissociation is in order. The diatomic molecule's rotation is designated by J, with N being its component that is perpendicular to the internuclear axis of symmetry. Radiative dipole transitions between lower (J'', N'') and upper (J', N') levels obey $\Delta J = J'–J'' = 0, \pm 1$. Such transitions are designated by a primary letter R, Q, or P for $\Delta J = +1, 0$, or -1, respectively. In addition, a superscripted S, R, Q, P, or O stand for $\Delta N = N'–N'' = +2$,

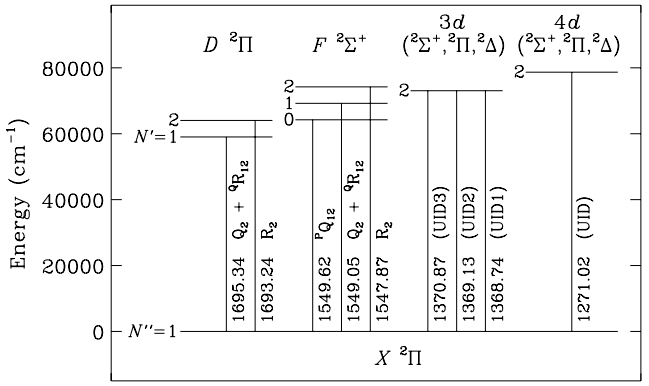

FIG. 1.—Term diagram for electronic states of CH discussed in this paper. The levels of each state are shown according to their N values, with a schematic not-to-scale energy separation. Only the lowest N' level is positioned at the correct location along the energy axis. This diagram shows only the transitions studied here. For the 1271.02 Å transition of the 4*d* Rydberg complex, we assumed that it has the same $N' = 2$ that has been assigned by Watson (2001) to the UID transitions of the 3*d* Rydberg complex.

+1, 0, −1, or −2, respectively. For $\Delta N = \Delta J$ transitions the superscripted letter will repeat the primary letter and is thus customarily omitted. Electronic states with angular momentum greater than 0, i.e., non-Σ states, interact with the nuclear spin to produce Λ-doubling of their rotational levels. Thus, the $X\ ^2\Pi$ ground state has two Λ-levels 0.11 cm^{-1} (1.4 km s^{-1}) apart, which are selectively connected by allowed transitions to upper states. Figure 1 indicates the transitions analyzed here. Owing to space limitations, Λ-levels and individual $J' = N' \pm 1/2$ levels are not shown, while N' level separations are shown in a highly magnified and schematic way. Since we show those levels involved with transitions discussed here, only the lowest N' level for each state is properly positioned with respect to the excitation energy axis. Once a transition to an upper electronic state has occurred, the strength of overlap between state wave functions determines the probability of radiationless predissociation. If the predissociation occurs via a state of similar electronic character, it is called homogeneous, and the rate will not vary strongly with J' of the predissociated state. Otherwise, heterogeneous predissociation occurs between states of differing characters, and a strong dependence on J' is observed.

2. DATA AND ITS MODELING

Our sample of 13 sight lines is obtained from spectra acquired with the Space Telescope Imaging Spectrograph (STIS) and the Goddard High-Resolution Spectrograph (GHRS). We analyzed the data, which are available from the *HST* archive, in order to derive 3*d*–*X f*-values for $\lambda\lambda$1368, 1369, and 1370 along 12 lines of sight. We obtained smaller samples of sight lines to be analyzed in the search for additional CH absorption features from its 4*d*–*X*, *F*–*X*, and *D*–*X* bands. Whenever multiple exposures were available, we combined them in wavelength space for an improved signal-to-noise ratio (S/N). In addition, when a feature (band) appeared in two adjacent orders, we combined them after correcting for any small wavelength inconsistencies. All our reductions were in IRAF[1] and STSDAS.[2]

Although it is known that the STIS line-spread function (LSF) possesses weak wings, we could not see any obvious signatures for such wings in the highest *R* data. (The fact that 3*d*–*X* λ1369 looks wider than other lines shows that this characteristic cannot be attributed to a global effect caused by prominent instrumental wings.) Therefore, we used a single Gaussian to describe the instrumental profile of STIS, in agreement with the findings of Jenkins & Tripp (2001). Nevertheless, the STIS handbook does show that the LSF wings have a larger role in the profile for wider slits. As a result, we did allow for *R* to be a fitted parameter during modeling of CO absorption lines (bands) taken from the same spectra used here. We found that *R* is lower for data taken through wider slits and vice versa. There is a good match between the range of resolving powers for a given slit and the range found by Bowers (1998). We will discuss these findings in a forthcoming publication about the CO molecule.

Table 1 provides a list of sight lines in terms of the star observed, its spectral type and Galactic direction, as well as the literature values for total W_{4300}(CH), total N(CH), and cloud structure fractions along each line of sight. For the first three sight lines, as well as the ninth, we use our latest N(CH) results based on modeling with Ismod.f (see below) of high-*R* (≈170,000)

[1] IRAF is distributed by the National Optical Astronomy Observatory, which is operated by the Association of Universities for Research in Astronomy, Inc., under cooperative agreement with the National Science Foundation.

[2] STSDAS is a product of the Space Telescope Science Institute, which is operated by AURA for NASA.

TABLE 1
STELLAR AND CH DATA FOR PROGRAM STARS

Star	Name	Sp.	l (deg)	b (deg)	W_{4300}(CH) (mÅ)	N_{tot}(CH) (10^{13} cm^{-2})	N_i(CH)/N_{tot}(CH)	CH Ref.
HD 23180	*o* Per	B1 III	160.36	−17.74	14.5 ± 0.5	1.90 ± 0.06	0.37, 0.63	1
HD 23478		B3 IV	160.76	−17.42	14.1 ± 0.5	1.83 ± 0.07	0.74, 0.26	1
HD 24398	ζ Per	B1 Iab	162.29	−16.69	15.7 ± 0.1	2.14 ± 0.01	0.56, 0.44	1
HD 24534	X Per	O9.5 pe	163.08	−17.14	26.3 ± 0.9	3.69 ± 0.13	0.14, 0.16, 0.70	2
HD 147683	V760 Sco	B4 V	344.86	+10.09	18.4 ± 2.2	2.22 ± 0.26	0.09, 0.68, 0.23	3
HD 149757	ζ Oph	O9 V	6.28	+23.59	19.6 ± 2.0	2.50 ± 0.25	0.50, 0.08, 0.42	4
HD 154368	V1074 Sco	O9 Ia	349.97	+3.22	38.7 ± 1.3	6.25 ± 0.21	0.03, 0.01, 0.03, 0.18, 0.70, 0.04, 0.01	2
HD 203374		B0 IVpe	100.51	+8.62	17.3 ± 1.0	2.22 ± 0.11	0.05, 0.04, 0.32, 0.20, 0.28, 0.06, 0.05	5
HD 203532		B3 IV	309.46	−31.74	18.0 ± 0.6	2.46 ± 0.08	0.40, 0.60	1
HD 207308		B0.5 V	103.11	+6.82	23.7 ± 1.0	3.21 ± 0.16	0.07, 0.09, 0.57, 0.27	5
HD 207538		O9 V	101.60	+4.67	28.0 ± 1.2	3.81 ± 0.19	0.06, 0.18, 0.31, 0.31, 0.11, 0.03	5
HD 208266		B1 V	102.71	+4.98	25.5 ± 1.2	3.35 ± 0.17	0.01, 0.39, 0.37, 0.12, 0.11	5
HD 210839	λ Cep	O6 Iab	103.83	+2.61	16.5 ± 1.7	2.08 ± 0.21	0.38, 0.62	4

NOTE.—We used the SIMBAD database for spectral types and Galactic coordinates.

REFERENCES.—(1) This paper; (2) D. E. Welty 2005, private communication; (3) Andersson et al. 2002; (4) Crane et al. 1995; (5) Pan et al. 2004.

TABLE 2
HST Spectroscopy of Program Stars

Star	Instr.	Data Set	Grating	Slit (arcsec)	S/N	$\lambda/\Delta\lambda$	CH Bands
HD 23180	STIS	o64801–4	E140H	0.2X0.05	100	120000	3*d*–*X*
HD 23478	STIS	o6lj01	E140H	0.1X0.03	30	130000	3*d*–*X*, *F*–*X*
HD 24398	STIS	o64810–11	E140H	0.2X0.05	90	120000	3*d*–*X*
HD 24534	STIS	o64812–13	E140H	0.1X0.03	105	140000	3*d*–*X*
	STIS	o66p01	E140H	0.2X0.09	85	100000	4*d*–*X*, 3*d*–*X*
	STIS	o66p02	E140H	0.2X0.09	55	100000	*F*–*X*
	STIS	o66p03	E140H	0.2X0.09	110	100000	*D*–*X*
HD 147683	STIS	o6lj06	E140H	0.2X0.09	35	120000	3*d*–*X*, *F*–*X*
HD 149757	GHRS	z0x201	G160M	0.25	900	20000	4*d*–*X*, 3*d*–*X*
	GHRS	z0hu01	G160M	2.0	110	15000	*F*–*X*
HD 154368	GHRS	z0wx02	G160M	0.25	30	20000	3*d*–*X*
HD 203374	STIS	o6lz90	E140M	0.2X0.2	45	40000	3*d*–*X*
HD 203532	STIS	o5c01s	E140H	0.2X0.2	25	80000	4*d*–*X*
HD 207308	STIS	o63y02	E140M	0.2X0.06	60	45000	4*d*–*X*, 3*d*–*X*, *F*–*X*
HD 207538	STIS	o63y01	E140M	0.2X0.06	55	45000	3*d*–*X*
HD 208266	STIS	o63y03	E140M	0.2X0.06	60	45000	3*d*–*X*
HD 210839	GHRS	z12j01	G160M	0.25	230	20000	3*d*–*X*
	GHRS	z2qx01–04	G160M	2.0	210	15000	*F*–*X*

optical spectra from McDonald Observatory. For the two stars in common, o Per and ζ Per, our results agree within 5% with those of Crane et al. (1995). A more detailed description of the new optical syntheses will be provided in a future publication. All N(CH) determinations to date have used the $A\,^2\Delta$–$X\,^2\Pi$ 4300.313 Å"line," which is a Λ-doublet of two R(1/2) transitions only 1.4 km s^{-1} apart (Black & van Dishoeck 1988). Table 2 lists the instrumental source for the VUV data, data set names, gratings, slits, S/N, fitted values for the spectral resolving power, R (from fits of CO absorption present in the same spectra), and CH bands detected in the *HST* data.

All line profiles analyzed in this paper were modeled by spectrum synthesis using the Y. S. code, Ismod.f. The basic radiative transfer equations in this code are taken from Black & van Dishoeck (1988). Fit parameters include radial velocity, N(CH), f-value, line width, and cloud component structure, which involves relative velocities, fractional abundances, and Doppler b-values. Both N(CH) and the cloud component structure were known a priori for each sight line and were kept fixed during the CH fits. Ismod.f employs the Voigt profile to describe the line shape as a combination of a Gaussian Doppler core and Lorentzian wings. The resulting profile is then convolved with the appropriate instrumental Gaussian profile before a comparison with the data is performed via rms computation. Ismod.f employs the simplex method to converge onto the final fit, which is found by an automated trial and error inspection of the parameter space in decreasing steps, until a certain tolerance level (usually 10^{-4} of the parameter's value) has been reached. Figure 2 shows the data and Ismod.f profile syntheses of the three 3*d*–*X* lines toward the star X Per.

3. INDIVIDUAL SIGHT LINES

We first compare a pertinent selection of our results with previously published values. Most of the work done previously concerned the well-known sight line toward ζ Oph. Our results from profile syntheses of $\lambda\lambda$1368, 1369, and 1370 show that fitted W_λ values for the three lines are 5.6 $\pm$ 0.2, 7.5 $\pm$ 0.2, and 2.2 $\pm$ 0.3 mÅ, respectively, where our uncertainties reflect noise contribution over the extent of the profile from the expression FWHM/(S/N). When compared to the two previous publications, our W_{1368} and W_{1370} agree more with Cardelli et al. (1991; 4.02 $\pm$ 0.58, 4.59 $\pm$ 0.74, and 1.16 $\pm$ 0.39 mÅ, respectively), while our W_{1369} agrees more with Tripp et al. (1994; 3.80 $\pm$ 0.80, 5.89 $\pm$ 0.89, and 0.84 $\pm$ 0.59 mÅ, respectively). It is possible that our W_λ values are larger, because they include more of the contribution of the wide wings that arise in predissociation. When wide wings are unknowingly present, their depression of the local continuum might be assumed to arise in the continuum itself (e.g., owing to stellar undulations). Special care should be taken to preserve such wings during the rectification process, but this is hard to accomplish for data with low S/N.

Gnaciński et al. (1997) measured W_{1369} toward six stars, of which three sight lines are in common with this study. Therefore,

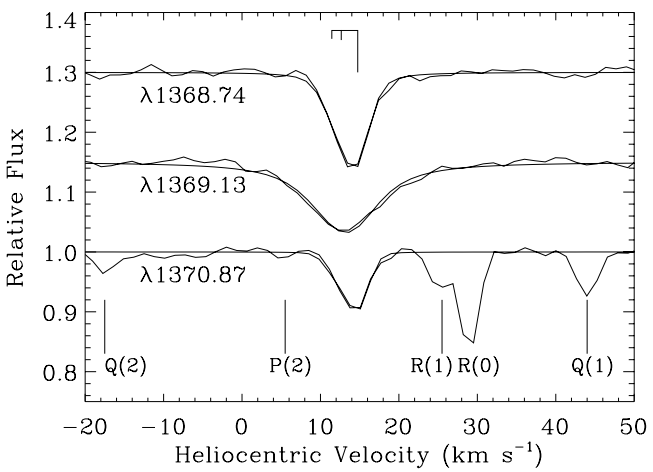

Fig. 2.—Data and fits for $\lambda\lambda$1368, 1369, and 1370 from the 3*d*–*X* band of CH toward X Per, vertically separated by 0.15 continuum units. This set of data is of higher R and S/N than the spectrum used in the initial detection of these lines toward ζ Oph. In addition, N(CH) is higher along the X Per sight line, which shows a three-cloud component structure as indicated by the fraction-scaled pointers above the spectra. The larger width of λ1369 is obvious. Its slight blueshift relative to λ1368 and λ1370 shows that its rest wavelength should be adjusted by ≈ -0.005 Å relative to the sharper lines. The line λ1370 is located among lines from ^{13}CO; those to the blue are from the A–X (6–0) band, while those to the red are from the d–X (12–0) intersystem band (see Fig. 1 of Sheffer et al. 2002).

TABLE 3
ASTRONOMICAL MEASUREMENTS OF $3d$–X LINES OF CH

	λ1368			λ1369			λ1370		
STAR	W_λ (mÅ)	f-Value (10^{-3})	$k_{pr}/10^{11}$ (s^{-1})	W_λ (mÅ)	f-Value (10^{-3})	$k_{pr}/10^{11}$ (s^{-1})	W_λ (mÅ)	f-Value (10^{-3})	$k_{pr}/10^{11}$ (s^{-1})
HD 23180	3.1 ± 0.2	20 ± 1	1.1	5.7 ± 0.5	39 ± 4	4.3	1.1 ± 0.2	7 ± 1	0.10[a]
HD 23478	2.9 ± 0.7	20 ± 5	1.6	3.9 ± 0.7	26 ± 5	2.3	1.5 ± 0.7	10 ± 5	0.09
HD 24398	2.3 ± 0.2	15 ± 1	1.0[a]	4.4 ± 0.4	27 ± 2	3.9	1.6 ± 0.2	9 ± 1	0.06
HD 24534	4.7 ± 0.1	16 ± 1	0.8	8.0 ± 0.3	29 ± 2	3.8	2.2 ± 0.2	8 ± 1	0.17
HD 147683	4.5 ± 0.8	25 ± 5	0.8	6.5 ± 1.7	38 ± 11	4.7	1.6 ± 0.4	9 ± 3	0.10[a]
HD 149757[b]	5.6 ± 0.2	29 ± 3	2.1	7.5 ± 0.2	39 ± 4	3.9	2.2 ± 0.3	11 ± 2	0.10[a]
HD 154368[b]	11.3 ± 1.2	24 ± 3	1.7	17.2 ± 2.0	37 ± 5	4.1	...	...	...
HD 203374	3.4 ± 1.2	19 ± 7	1.5	5.2 ± 1.8	30 ± 10	3.3	...	...	...
HD 207308	4.7 ± 1.0	19 ± 4	2.3	5.7 ± 1.0	23 ± 4	3.8	2.5 ± 0.4	10 ± 2	0.10[a]
HD 207538	5.5 ± 0.7	18 ± 2	2.4	9.0 ± 1.3	31 ± 5	4.0	2.9 ± 1.4	10 ± 5	0.10[a]
HD 208266	4.8 ± 0.7	18 ± 3	1.7	6.9 ± 1.2	27 ± 5	3.9	2.4 ± 0.5	9 ± 2	0.10[a]
HD 210839[b]	5.4 ± 0.5	33 ± 4	1.0[a]	7.5 ± 0.5	47 ± 6	3.6	1.7 ± 0.5	10 ± 3	0.10[a]
STIS avg.		19 ± 3	1.5 ± 0.6		30 ± 5	3.8 ± 0.7		9 ± 1	0.11 ± 0.06

[a] These are fixed, not fitted, k_{pr} values.
[b] These GHRS data are not included in the STIS average.

we may compare our synthesized W_λ values (in milliangstroms) with those of Gnaciński et al.: X Per, 8.0 ± 0.3 versus 8.4; ζ Oph, 7.5 ± 0.2 versus 6.3; and λ Cep, 7.5 ± 0.5 versus 6.9. There are no major disagreements between the two sets of values. Note that for the ζ Oph sight line, the value from Gnaciński et al. is also higher than those from Cardelli et al. (1991) and Tripp et al. (1994).

Federman et al. (1995) have been the only authors to report the presence of the λ1271 feature, in the direction of ζ Oph. Their reported value was $W_\lambda = 0.75 \pm 0.19$ mÅ, while our fitted result is 1.1 ± 0.1 mÅ. The latter agrees within 2 σ of the earlier value.

4. THE $3d$–X $^2\Pi$ BAND OF CH

4.1. *Oscillator Strengths*

An absorption line is produced by the combined action of N absorbers per square centimeter along the line of sight, each removing photons from the beam at the transition wavelength (λ in angstrom) at a rate that corresponds to an oscillator strength, or f-value. The mutual product fN appears in the equation that determines the optical depth in the transition, which then generates the W_λ of the line profile through exponential absorption along the line of sight. It is customary to have at hand transitions with known f-values that, consequently, allow the determination of N of the absorbers. Here, on the other hand, we use the known values of N(CH) from 12 sight lines to determine the f-values for λλ1368, 1369, and 1370.

Table 3 provides the results of our spectrum syntheses for the three $3d$–X lines toward our target stars, fitted W_λ, f-values and inferred intrinsic Lorentzian line widths (see more about the width in § 4.2). Normally, N(CH) is determined from the A–X doublet of $J'' = 1/2$ transitions at 4300.313 Å, where the two blended Λ-levels have their populations combined. Indeed, ultrahigh-R spectra at 4300 Å (e.g., Lambert et al. 1990) sometimes resolve the 1.4 km s^{-1} doublet, revealing equal populations for the two components. Here, we emphasize that each of our profile syntheses employs only half the value of N(CH) (taken from Table 1), because in all resonance transitions to higher (than A) electronic states of CH, the individual Λ-components are well separated (see Lien 1984). Therefore, the f-values derived here are twice as large as they would have been had the full value of N(CH) been used. Within the uncertainties listed, there is good agreement among all sight lines for each f-value. Nonweighted means for the three lines are $f(1368) = 0.019 \pm 0.003$, $f(1369) = 0.030 \pm 0.005$, and $f(1370) = 0.009 \pm 0.001$. For these averages we used fit results from the higher R STIS spectra, while avoiding two (in the case of λ1370) or three (otherwise) sight lines from lower R GHRS exposures. Low-R data do not provide as good a handle on intrinsic line profiles as do high-R data, both in the reduction (i.e., continuum rectification) stage and in the modeling stage. Had we used the excluded results, the average f-values would have increased by 11%, 10%, and 3%, respectively. Thus the sum of the STIS-derived f-values for the three transitions is 0.058 ± 0.006, which according to Watson (2001) is providing some 76% of the total f-value of the $3d$–X band, because the three lines are the most prominent transitions in it. With the correction, this Rydberg band has a total f-value of 0.076 ± 0.008, as inferred by our interstellar measurements.

Watson (2001) derived a preliminary f-value for the $3d$–X band from the sum of W_λ of the three lines in Tripp et al. (1994; 10.5 mÅ), employing $N(\mathrm{CH}) = 10^{13.4}$ cm^{-2} from Federman & Lambert (1988) and the expression for unsaturated line absorption, $\log(W_\lambda/\lambda) = \log(f\lambda) + \log(N) - 20.053$, from Morton & Noreau (1994). From this value, $f = 0.025$, which was not based on any profile spectral synthesis, Watson (2001) estimated the total band f-value to be 0.033. (We estimate that the uncertainties associated with Watson's f-values amount to 20%, based on the W_λ uncertainties in Tripp et al.) Both values appear to be too low by a factor of 2.3 ± 0.5 when compared to our results. However, Watson's determination was based on the full value of the N(CH), whereas in our modeling we use N(CH)/2, which is pertinent for the population of a single Λ-doubling level, see above. Correcting Watson's estimate upward by a factor of 2, we get $f \approx 0.050 \pm 0.010$ for the sum of three lines, and $f \approx 0.066 \pm 0.013$ for the entire $3d$–X band. This happens to be in much better agreement with our rigorous spectrum synthesis results. Only two theoretical ab initio band f-values exist in the literature: 0.0467 (not 0.0362 as per Watson [2001]) from Barsuhn & Nesbet (1978) and 0.069 from van Dishoeck (1987). It appears that both our astronomically derived band f-value, and the Watson

(2001) value, when corrected upward by a factor of 2, are in good agreement with the theoretical value calculated by van Dishoeck (1987), thus bolstering the case for identifying these three lines with the CH molecule. This measurement also shows $3d$–X to be the CH band with the largest f-value. Perhaps this is what Herzberg & Johns (1969) meant when they commented that G–X lines would be the strongest interstellar lines of CH.

4.2. *Predissociation Widths*

As mentioned in § 4.1, Table 3 provides information about the Lorentzian line width derived in our modeling. The intrinsic line width is set by the lifetime of the transition's upper level, according to the inverse quantum mechanical relationship between lifetime (limiting the interval of measurement) and line width (resulting uncertainty in measured energy). Normally, intrinsic line widths are unobservable owing to the relatively "long" lifetimes of radiative transitions; $\tau \geq 10^{-8}$ s yields a width of 0.01 mÅ or less, using the relationship $\Gamma(\text{mÅ}) = [\lambda(\text{Å})]^2/(1.884 \times 10^{16}\tau)$. Predissociation generates much shorter lifetimes for certain Rydberg states, owing to decay rates that may readily be 10^3 times faster than radiative decay rates. Under such circumstances, the associated lifetime would be 10^{-11} s, leading to line widths of the order of 10 mÅ, which can be measured on high-R (≈100,000) spectra with the help of profile synthesis. We estimate that in our highest R data it is possible to reliably extract Γ widths of a few mÅ, which correspond to decay rates that are higher than a few $\times 10^{10}$ s^{-1}. For f-value syntheses that failed to converge onto a reliable Γ solution, we fixed the line width to a value near the average from well-converged solutions. The predissociation decay rate, $k_{\rm pr}$, is the inverse of τ and, thus, is directly proportional to Γ. We use both $k_{\rm pr}$ and Γ as descriptors of line width in terms of Lorentzian wings.

Modeling the three $3d$–X lines with Ismod.f returned values for the Lorentzian width in inverse lifetimes (s^{-1}), which are tabulated in Table 3. We computed the means from all sight lines with high-R (non-GHRS) determinations and derived the following predissociation rates: $k_{\rm pr}(1368) = (1.5 \pm 0.3) \times 10^{11}$, $k_{\rm pr}(1369) = (3.8 \pm 0.7) \times 10^{11}$, and $k_{\rm pr}(1370) = (1.1 \pm 0.6) \times 10^{10}$ s^{-1}. It can be seen that all data sets returned a well-defined line width for λ1369, thanks to its larger Γ, but that only a few syntheses were successful in converging onto a Γ solution for λ1370, the profile with the narrowest wings. In fact, whereas average $k_{\rm pr}$ values for both λ1368 and λ1369 are better than the 2.5 σ detection level, $k_{\rm pr}$ for λ1370 is a <2 σ result. It is thus possible that the width of λ1370 has not been reliably determined, and that a 3 σ upper limit of $\approx 3 \times 10^{10}$ s^{-1} for $k_{\rm pr}(1370)$ should be used instead.

According to the Γ-τ relationship, the corresponding Lorentzian profile widths of the three $3d$–X lines are 11.6, 38.4, and 1.1 mÅ, which correspond to 0.62, 2.05, and 0.06 cm^{-1}. Watson (2001) used the value 2.6 cm^{-1} for the width of λ1369, which was based on the value of 10.7 km s^{-1} in Tripp et al. (1994). We also note that the original observation of λ1369 toward ζ Oph was described as showing an asymmetric profile. Here, our impression from the entire sample of sight lines is that the observed profiles of λ1369 are very consistent with formation by a single transition, i.e., there are no indications for asymmetries in the line profile, especially in higher R data.

Theory has no definite bearing on these $k_{\rm pr}$ values, yet. Van Dishoeck (1987) remarked that although predissociation is present in all bands studied by Herzberg & Johns (1969) for most bands, including the $3d$–X band at 1370 Å, it is heterogeneous. Thus, the predissociation rate may approach an estimated value of 10^{10} s^{-1} for $N' = 10$ but is estimated to be about 10^8 s^{-1} for low N', i.e., of the order of the radiative decay rate of the state. These estimates are not rigorous enough to be more accurate that an order of magnitude. Indeed, our fits and Watson's initial probe do show that in the case of both λ1368 and λ1369 there is a substantial contribution to CH photodissociation, since their $k_{\rm pr}$ values are much higher than what van Dishoeck (1987) had suggested. According to Watson (2001) all three lines are $N' = 2$ transitions.

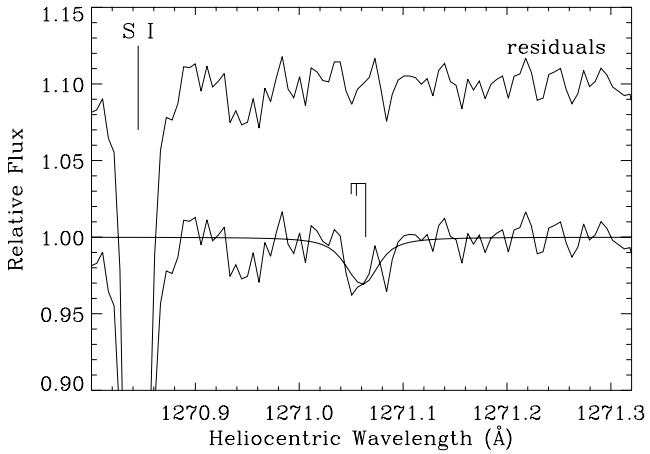

FIG. 3.—Data, fit, and residuals for λ1271 from the $4d$–X band of CH toward X Per. The cloud component structure on the line of sight is indicated above the fit. The strong absorption to the blue is from a triplet of S I lines at 1270.78 Å.

Figure 2 shows that there is good agreement between our models and observed line profiles. For λ1369, there is no need to invoke an analogy to the DIBs in the optical, because we see that very good fits are obtained using a single transition with broad predissociation Lorentzian wings. In addition to agreeing with Watson (2001) that CH is a very good assignment for λλ1368, 1369, and 1370, one may also conclude that VUV analogs of the optical DIBs have yet to be detected.

5. THE $4d$–X $^2\Pi$ BAND OF CH

Our inspection of archival STIS data returned four candidate sight lines with λ1271 features that appear to be astronomical detections of the strongest transition in $4d$–X. The sight lines are toward X Per (shown in Fig. 3), ζ Oph, HD 203532, and HD 207308, as listed in Table 4. Despite varying values of S/N and R, all four spectrum syntheses returned rather consistent solutions, $f = 0.007 \pm 0.002$. This f-value is smaller than that for λ1369, the strongest $3d$–X transition with f of 0.030 ± 0.005 reported above. A theoretical prediction from Barsuhn & Nesbet (1978) gives f-values of 0.0198 and 0.0186 for the $^2\Delta$ and $^2\Pi$ states in the $4d$ complex, respectively. If we assume that the total band f-value is 2.5 times the value of its strongest transition, as we find for the $3d$–X band complex and λ1369, then from the f-value for λ1271 we expect $f \approx 0.0175$ for the entire $4d$–X band. This value is in close agreement with the predictions of Barsuhn & Nesbet for a single ($^2\Delta$ or $^2\Pi$) state only, falling short by a factor of 2 relative to their sum. Van Dishoeck (1987) did not include the $4d$ state in her f-value calculations.

However, van Dishoeck suggested that $k_{\rm pr}(4d)$ would be smaller than that of the $3d$ state owing to a smaller overlap of the $4d$ state with the nuclear wave functions. Three sight lines with either the highest R or the highest S/N values yielded solutions for Γ, while for HD 207308 the fit did not converge onto a reliable Lorentzian line width. With an average of $k_{\rm pr} = (2.5 \pm 1.5) \times 10^{11}$ s^{-1}, this transition has a predissociation rate between those of λ1368 and λ1369. Owing to small number ($n = 3$) statistics, this <2 σ result

TABLE 4
ASTRONOMICAL MEASUREMENTS OF $4d$–X, F–X, AND D–X LINES OF CH

Star	W_λ (mÅ)	f-Value (10^{-3})	$k_{pr}/10^{11}$ (s^{-1})	W_λ (mÅ)	f-Value (10^{-3})	$k_{pr}/10^{11}$ (s^{-1})	W_λ (mÅ)	f-Value (10^{-3})	$k_{pr}/10^{11}$ (s^{-1})
	$4d$–X λ1271			F–X 1549.05 Å[a]			F–X 1549.62 Å		
HD 23478	...	...	...	5.2 ± 1.6	28 ± 9	2.0[b]	...	...	...
HD 24534	1.6 ± 0.3	6 ± 1	3.1	6.3 ± 0.9	17 ± 2	3.0	3.9 ± 0.4	11 ± 1	0.6
HD 147683	...	...	...	6.6 ± 1.6	29 ± 7	2.0[b]	2.6 ± 1.5	15 ± 9	2.0[b]
HD 149757	1.1 ± 0.1	6 ± 1	3.5	4.1 ± 0.9	16 ± 4	2.5	4.4 ± 0.8	16 ± 3	2.5[b]
HD 203532	1.3 ± 0.5	7 ± 3	0.8	...	...	...	...	...	...
HD 207308	2.2 ± 0.7	10 ± 3	3.0[b]	4.6 ± 0.7	14 ± 2	1.1	3.1 ± 0.9	9 ± 3	1.0[b]
HD 210839	...	...	...	4.2 ± 0.6	21 ± 3	4.3	3.0 ± 0.5	14 ± 3	2.5
Average		7 ± 2	2.5 ± 1.5		21 ± 6	2.7 ± 1.3		13 ± 3	1.6 ± 0.9
	D–X λ1693			D–X λ1695[a]					
HD 24534	0.6 ± 0.3	1.2 ± 0.6	0.7[b]	1.8 ± 0.5	3.8 ± 1.1	0.7			
HD 24534[c]	0.8 ± 0.4	1.9 ± 1.0	3.6[b]	2.5 ± 1.0	5.7 ± 2.3	3.6[b]			

[a] These features are known to be blends of Q_2 and $^QR_{12}$, see text.
[b] These are fixed, not fitted, k_{pr} values.
[c] This D–X synthesis for HD 24534 incorporates the laboratory value of Γ (see text and Figs. 5 and 6).

seems to suffer from either noise and/or continuum biases. Furthermore, because only a single $J'' = 1/2$ transition has been found so far, the detection of $4d$–X is not as secure as those of the other CH bands described here.

6. THE $F\ ^2\Sigma^+$–$X\ ^2\Pi$ BAND OF CH

Herzberg & Johns (1969) observed this band at 1549 Å, i.e., it is located between the two components of the C IV doublet $\lambda\lambda$1548, 1550 seen in stellar and interstellar spectra. They noticed an increasing diffuseness with higher J, signaling heterogeneous predissociation. We detected two $J'' = 1/2$ absorption features from the F–X band along the sight lines toward X Per (see Fig. 4), HD 147683, ζ Oph, HD 207308, and λ Cep, as listed in Table 4. The redder, weaker line at 1549.62 Å belongs to a single transition, $^PQ_{12}$, while the stronger line at 1549.05 Å is an unresolved blend of the two transitions Q_2 and $^QR_{12}$. According to Lien (1984) who analyzed the $C\ ^2\Sigma^+$–$X\ ^2\Pi$ band of CH, both Q_2 and $^PQ_{12}$ have a Hönl-London factor (HLF) of 4/3, while $^QR_{12}$ has HLF = 2/3. (Since the F state is also of a $^2\Sigma^+$ character, the same HLFs should apply in F–X and C–X transitions.) The line of sight toward HD 23478 shows only the strongest feature from the F–X band, i.e., the blend λ1549.

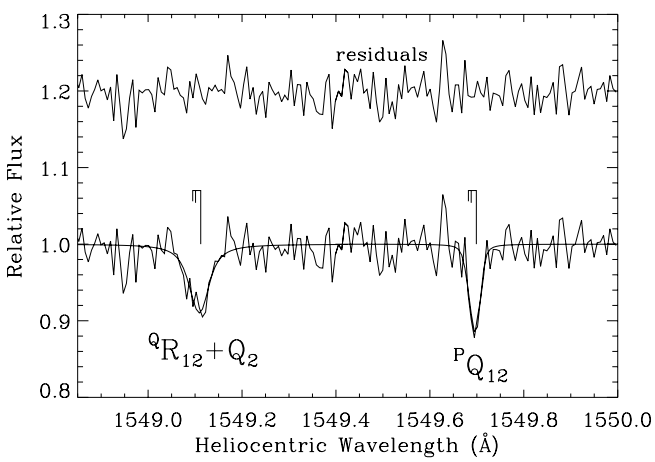

FIG. 4.—Data, fits, and residuals for 1549.05 and 1549.62 Å from the F–X band of CH toward X Per. The bluer "line" is a blend of two transitions, Q_2 and $^QR_{12}$, but their separation is unknown. The redder line is the unblended $^PQ_{12}$ transition. The cloud component structure is indicated above the features.

The averages of our fitted f-values, based on the known values of $N(\mathrm{CH})/2$, are $f(1549.05) = 0.021 \pm 0.006$ and $f(1549.62) = 0.013 \pm 0.003$. The f-value ratio is 1.6 ± 0.6 for 1549.05 Å versus 1549.62 Å. Based on the actual transitions that constitute these lines and their individual HLF values, the predicted f-value ratio is 1.5, showing good agreement with our measurements. The total f-value of 1549.05 Å equals the total band f-value, according to the sum of HLFs, or $4/3 + 2/3 = 6/3$. Here we derive a sum of $f = 0.021 \pm 0.006$, whereas Barsuhn & Nesbet (1978) and van Dishoeck (1987) theoretically computed values of 0.031 and 0.0095, respectively. Our value lies between the predicted f-values, about a factor of 2 from either one.

There is another potentially detectable $J'' = 1/2$ absorption line belonging to the F–X band, R_2 at 1547.87 Å (Herzberg & Johns 1969). We were not able to detect it owing to blending with the blue wing of the much stronger line of C IV at 1548.204 Å. According to its HLF of 2/3, the R_2 transition would constitute the weakest $J'' = 1/2$ absorption line. Since we measure two lines composed of the three strongest transitions with verified f-value ratios, these first astronomical detections of the F–X band of CH seem secure.

We also extracted Lorentzian widths for the absorption lines of the F–X band, as listed in Table 4. As is the case for the lines of the $3d$–X band, under conditions of high-R the lines readily show that different predissociation widths are involved, confirming the Herzberg & Johns (1969) observation of heterogeneous predissociation for F–X. In a similar fashion to $3d$–X, the strongest line in the band also appears to be the widest. Thus, for the blend $Q_2 + ^QR_{12}$ at 1549.05 Å, we find $k_{pr} = (2.7 \pm 1.3) \times 10^{11}\ s^{-1}$, whereas k_{pr} for $^PQ_{12}$ at 1549.62 Å is $(1.6 \pm 0.9) \times 10^{11}\ s^{-1}$. A golden rule approximation by van Dishoeck (1987) yielded a computed k_{pr} of $7.6 \times 10^9\ s^{-1}$ for the $N' = 1$ levels of the F state, with a stated uncertainty of "an order of magnitude." The two transitions with $N' = 1$ (Q_2 and $^QR_{12}$) are those that make up the blend at 1549.05 Å, for which we find k_{pr} that is larger by 1.5 orders of magnitude than the approximate prediction.

We attempted a more detailed spectrum synthesis of 1549.05 Å toward X Per that explicitly included the two transitions Q_2 and $^QR_{12}$, subject to the constraint of a 2:1 ratio in their HLF values.

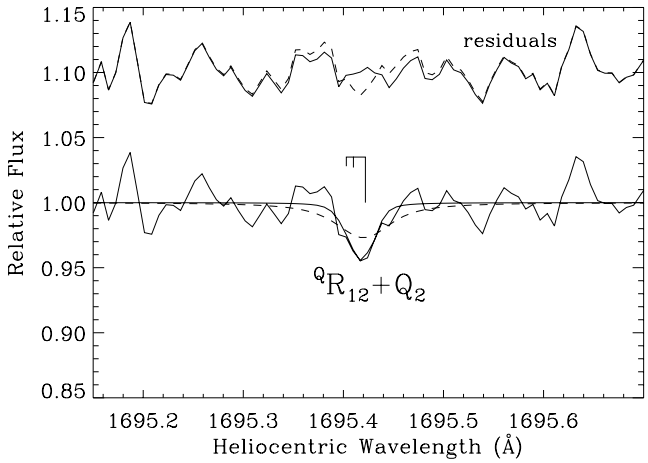

FIG. 5.—Data, fits, and residuals for λ1695 from the D–X band of CH toward X Per. This is a blend of the two transitions, Q_2 and $^{Q}R_{12}$, the separation of which is unknown. The cloud component structure is indicated above the fitted feature. Our initial fit returned a line of smaller width (*solid line*) than the value measured in the lab (*dashed line*), yet both are consistent with the ambient noise in the spectrum.

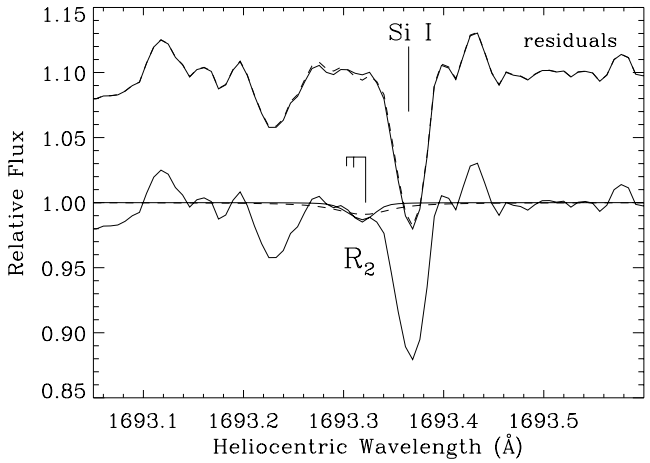

FIG. 6.—Data, fits, and residuals for λ1693 from the D–X band of CH toward X Per. This is the weaker transition R_2, which is partially blended with the Si I at 1693.29 Å. The cloud component structure is indicated above the fitted line. Both fits employ fixed Γ values from the λ1695 fits in Fig. 5. The feature at $\sim$1693.25 Å does not appear in any tabulated interstellar line list.

Although the fit returned a separation of -6.2 km s^{-1} for the weaker $^{Q}R_{12}$ relative to Q_2, we take this to be an upper limit, because the fit yielded a solution with residuals that are somewhat smaller that the ambient noise level away from the feature. The actual energy level splitting in the $F\,^2\Sigma^+$ state that controls the velocity separation between the two 1549.05 Å transitions is unknown, but we note that the C–X band has its $^{Q}R_{12}$ line located 2.2 km s^{-1} to the blue of Q_2 (Lien 1984).

This detailed synthesis of the $Q_2 + ^{Q}R_{12}$ blend resulted in narrower Lorentzian wings for the two transitions and (predictably) lower f-values relative to the single-transition model. It returned $f(Q_2) = 0.010$ and $f(^{Q}R_{12}) = 0.005$, i.e., a sum that is 12% smaller than the f-value fitted for the entire blend, and decay rates $k_{\rm pr} = 1.3 \times 10^{11}$ and 1.1×10^{11} s^{-1}, for Q_2 and $^{Q}R_{12}$, respectively. These lower $k_{\rm pr}$ values are still higher than the approximate prediction of van Dishoeck (1987). The similarity in decay rates for the two transitions is inconsistent with their J' levels of 1/2 (for Q_2) and 3/2 (for $^{Q}R_{12}$), because heterogeneous predissociation is normally revealed by Γ having a dependence on $J(J+1)$, i.e., we expect $^{Q}R_{12}$ to be 5 times wider than Q_2. Since detailed modeling attempts for other sight lines did not return separations and widths for the blended components that were in good agreement with the X Per result, the quality of the data must be insufficient for such detailed modeling, especially when the line separation is not available as a known input value.

7. THE $D\,^2\Pi$–$X\,^2\Pi$ BAND OF CH

This band was observed by Herzberg & Johns (1969) who remarked on the relative weakness of its Q-branch and the apparent diffuse nature of its lines. A single sight line, that toward X Per, exhibits an absorption feature that is consistent with a detection of the line at 1695.34 Å, the strongest feature in D–X (see Fig. 5 and Table 4). Here the strongest feature is also an unresolved blend of the two transitions Q_2 and $^{Q}R_{12}$ (Krishna Swamy & Tarafdar 1973). Furthermore, a shallower feature in the spectrum is consistent with the position of the R_2 1693.24 Å transition of D–X, although it is partially blended with a stronger Si I λ1693 line (see Fig. 6). Upon modeling, the known N(CH)/2 toward X Per returns f-values of 0.0038 ± 0.0011 and 0.0012 ± 0.0006 for $Q_2 + ^{Q}R_{12}$ and R_2, respectively, while the ratio of their f-values is 3.2 ± 1.8. Krishna Swamy & Tarafdar (1973) theoretically predicted a 5 : 1 ratio for λ1695 versus λ1693, a value that is consistent with our determinations. Theoretical computations by van Dishoeck (1987) gave $f = 0.0073$ for the 0–0 band of the $^2\Pi_1$ state, which she identified with the D state. Barsuhn & Nesbet (1978) calculated a value of 0.0010 for $f(D$–$X)$. Our value of 0.0038 ± 0.0011 for the strongest feature appears to be within a factor of 2–3 of the two quantum mechanical predictions. In light of the good agreement in wavelength and f-value with predicted values, we have high confidence in treating this case as the first astronomical detection of the D–X band from CH.

Concerning Lorentzian line width, our synthesis of the blend at λ1695 returned $k_{\rm pr} = 7.0 \times 10^{10}$ s^{-1}, a rate that was kept fixed during the modeling of the partially blended R_2 line. However, Li & Lee (1999) measured decay rates of $(3.6 \pm 0.6) \times 10^{11}$ s^{-1} in the laboratory for the $N' = 2$ levels of D–X, and Metropoulos & Mavridis (2000) calculated a lifetime of 1.6 ps for the same state, albeit they denoted it by the letter E. These consistent nonastronomical values show that predissociation dominates the decay of D levels, as happens for the 3d levels. Consequently, we resynthesized λ1695 with a fixed input Γ value from Li & Lee (1999) yielding $f = 0.0057 \pm 0.0023$, which is in good agreement with the calculated value of 0.0073 from van Dishoeck (1987). Likewise, the f-value of λ1693 also increased by about 50%; see Table 4. According to Figure 5, it seems that owing to insufficient S/N, our original fit of λ1695 had converged onto a solution involving a noise glitch, leading to a $k_{\rm pr}$ value that was too small. The revised fits with the terrestrial value for Γ are also consistent with the data.

8. CONCLUSIONS

We surveyed a sample of interstellar sight lines and specific spectral ranges to search for new astronomical detections of VUV transitions of the CH molecule, as well as to confirm the Watson (2001) identification of four UID lines as transitions involving two Rydberg states of CH. We found that both old and new detections appear to be consistent with the identification of CH as their source, based on known amounts of CH along the lines of sight, on predicted wavelength positions, and on theoretical f-values. Thus the decades-long tradition of optical observations of CH, using its A–X, B–X, and C–X bands, can now be

extended into the VUV via observations of its D–X, F–X, and $3d$–X (G–X) bands and, more reservedly, the $4d$–X band.

We could not find any absorption features that might be identified with E–X transitions of CH, listed by Herzberg & Johns (1969) to be near 1557 Å. This band is problematic with an unknown configuration, and could be arising either from an $E\ ^2\Pi$ state or it could be the 2–0 band of D–X (Chen et al. 1985), which has a very low f-value of 3.0×10^{-6} (van Dishoeck 1987) and a very high rate of predissociation, $k_{\rm pr} = 1.4 \times 10^{13}$ s^{-1} (Metropoulos & Mavridis 2000). Both characteristics of extremely weak oscillator strengths and extremely wide line profiles would easily render this band undetectable in astronomical or low-N(CH) settings.

Finally, with the confirmation that wider-than-average line profiles are attributable to high predissociation rates and symmetric Lorentzian wings in Rydberg transitions of CH, there are no candidates currently left in the VUV spectral regime that may be associated with the famous optical DIB bands.

We acknowledge support from NASA (grants NAG 05-11440 and NNG 06-GC70G) and the Space Telescope Science Institute (grant HST-AR-09921.01-A). We thank D. Welty for providing us with CH cloud structures toward X Per and HD 154368 prior to publication and an anonymous referee for helpful comments.

REFERENCES

Andersson, B-G, Wannier, P. G., & Crawford, I. A. 2002, MNRAS, 334, 327
Barsuhn, J., & Nesbet, R. K. 1978, J. Chem. Phys., 68, 2783
Black, J. H., & van Dishoeck, E. F. 1988, ApJ, 331, 986
Bowers, C. W. 1998, in 1997 HST Calibration Workshop, ed. S. Casertano et al. (Baltimore: STScI), 18
Cardelli, J. A., Savage, B. D., & Ebbets, D. C. 1991, ApJ, 383, L23
Chen, P., Chupka, W. A., & Colson, S. D. 1985, Chem. Phys. Lett., 121, 405
Crane, P., Lambert, D. L., & Sheffer, Y. 1995, ApJS, 99, 107
Eidelsberg, M., Sheffer, Y., Federman, S. R., Lemaire, J. L., Fillion, J. H., Rostas, F., & Ruiz, J. 2006, ApJ, 647, 1543
Federman, S. R., Cardelli, J. A., van Dishoeck, E. F., Lambert, D. L., & Black, J. H. 1995, ApJ, 445, 325
Federman, S. R., & Lambert, D. L. 1988, ApJ, 328, 777
Gnaciński, P., Sikorski, J., & Kaczmarczyk, G. 1997, Acta Astron., 47, 225
Herzberg, G., & Johns, J. W. C. 1969, ApJ, 158, 399
Jenkins, E. B., & Tripp, T. M. 2001, ApJS, 137, 297
Krishna Swamy, K. S., & Tarafdar, S. P. 1973, A&A, 28, 99
Lambert, D. L., Sheffer, Y., & Crane, P. 1990, ApJ, 359, L19
Li, X., & Lee, Y.-P. 1999, J. Chem. Phys., 111, 4942
Lien, D. J. 1984, ApJ, 284, 578
Metropoulos, A., & Mavridis, A. 2000, Chem. Phys. Lett., 331, 89
Morton, D. C., & Noreau, L. 1994, ApJS, 95, 301
Pan, K., Federman, S. R., Cunha, K., Smith, V. V., & Welty, D. E. 2004, ApJS, 151, 313
Sheffer, Y., Federman, S. R., & Lambert, D. L. 2002, ApJ, 572, L95
Tripp, T. M., Cardelli, J. A., & Savage, B. D. 1994, AJ, 107, 645
van Dishoeck, E. F. 1987, J. Chem. Phys., 86, 196
Viala, Y. P., Letzelter, C., Eidelsberg, M., & Rostas, F. 1988, A&A, 193, 265
Watson, J. K. G. 2001, ApJ, 555, 472